Ballistic performance of Polycarbonate and Polymethylmethacrylate under normal and inclined dynamic impacts

Shabnam Sadeghi Esfahlani[a,*]

[a]*Anglia Ruskin University, Engineering and the Built Environment, CM1 1SQ, Chelmsford, Essex, United Kingdom*

Abstract

Polymeric materials have exceptional mechanical properties, making them attractive for automotive, aerospace, defence and buildings industries. The numerical analysis of translucent polymeric materials' ballistic performance is investigated to analyse the deflection and perforation performance at high impact velocities. Computational methods are exploited to predict the ballistic performance of thick targets and projectile damage, and the results are validated against published works. The 3D numerical analysis is conducted by simulating plates and projectiles' mechanical performance that controls the deflection and ricochet procedure. Impact damage analysis is undertaken on monolithic Polycarbonate (PC) and Polymethylmethacrylate (PMMA) targets under various impact velocities, projectile's core density with inclined 30° and normal 90° impact angle. The results are analysed in terms of failure performance, depth of penetration (DOP), penetration path (POP), and residual velocity. The numerical analysis is further developed to study the effects of projectile impact velocity on the DOP and its direction. It is found that the DOP scales linearly with the impact velocity, where the POP is still nonlinear. Extended Drucker Prager Strength (EDP) material model with the failure criteria of principal stress and tensile pressure failure is used to simulate the brittle-ductile PMMA target's performance under dynamic impact. Shock Hugoniots equation of state with plastic strain failure is conducted to affect PC plates' tensile performance.

1. Introduction

Polymers are essential in a variety of engineering applications for their outstanding mechanical properties, in particular, excellent strength to weight ratios [1]. These materials have rate-dependent mechanical properties, low cost, and high durability [17]. The ballistic performance of amorphous polymers at high speed has a significant role in designing protective structures, such as military, nuclear reactor vessels, and bulletproof shields. Three critical properties can be assigned to glassy polymers, including high dynamic compressive strength, high brittleness and low density, as well as transparency, which is the characteristic of amorphous homopolymers [16]. The deformation mechanism of amorphous polymers is identified as thermally activated molecular movements processes described by the state transition theory, the conformational change theory, and the intermolecular shear resistance model [13]. The intermolecular shear resistance model depends on a specific range of temperatures and strain rates. There are two phases over a wide range of temperatures and strain rates while describing amorphous polymers' yield behaviour. Transition is associated with a sharp increase in yield stress and polymer chains' secondary relaxation with the precise molecular process. Various experimental studies have investigated the effect of compressive stress-strain of amorphous polymers such as PC and PMMA under different strain rates and temperatures. [20] showed that the α and β transition temperatures are closer to each other for the PMMA than those for the PC. The storage modulus value is an order of magnitude higher in the glassy state than in the rubbery state. [11] have done a uniaxial compression test and proposed constitutive relations to simulate glassy polymer's mechanical deformation. Their study showed some secondary molecular motion, distinct from molecular processes of the α transition, which has an independent contribution to the macroscopic rate dependence of these materials. [20] proposed two modifications to the constitutive relations of [11]. The constitutive relations claim a significant difference between numerical simulations' results with the consideration of plastic working and experimental results for uniaxial deformations at moderate and high strain rates. [20] has introduced two additional internal variables in the evolution equations for strain-softening to simulate the material's response at all strain rates more realistically. [12] presented the compressive experimental study of amorphous polymers under strain rates ranging ($10^{-4}s^{-1}$ to $5e^{3}s^{-1}$) and temperatures of ($40°C$ to $180°C$) where a modified Split-Hopkinson pressure bar was used to test materials under dynamic loading. [11] have conducted an experimental investigation of amorphous Polymers at various

*Corresponding author

Email address: shabnam.sadeghi-esfahlani@aru.ac.uk (Shabnam Sadeghi Esfahlani)

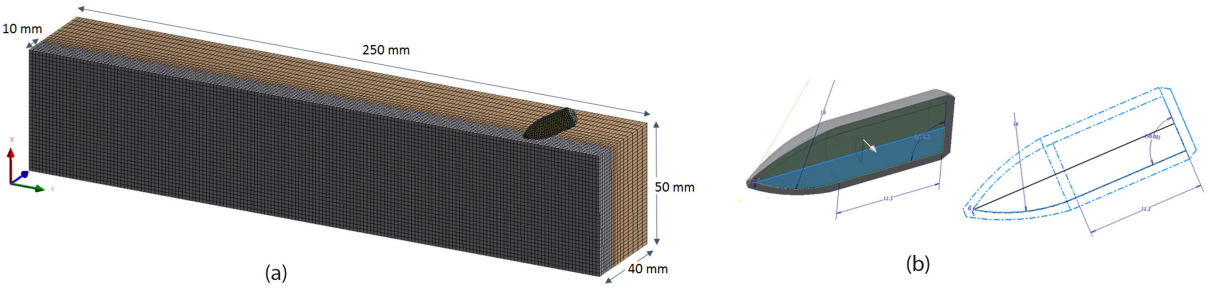

centring

Figure 1: (a) The half model of the projectile impacting a PMMA plate at an angle of inclination of 30°. (b) 0.3" bullet.

strain rates ranging from 10^{-4} s^{-1} to 10^{4} s^{-1}. They utilised the dynamic mechanical analyser tension test to characterise the viscoelastic behaviour, focusing on the rate-dependent shift of material transition temperatures. Uniaxial compression tests on the servo-hydraulic machine ranging 10^{-4} s^{-1} to s^{-1} and the split-Hopkinson pressure bar for 10^{3} s^{-1} to 10^{4} s^{-1} were used to characterize the rate-dependent yield and post-yield behaviour. The results have shown that temperature and strain rate significantly affect these materials' mechanical responses. An increasing strain rate will decrease the molecular mobility of the polymer chains by making the chains stiffer. It was illustrated that PC and PMMA exhibit increased yield rate sensitivity under the same strain rate conditions as the β transition of the viscoelastic behaviour. These experimental studies showed that during low to moderate rate compression testing on the servo-hydraulic instrument, both PC and PMMA specimens deform in a ductile manner up to a true strain of 0.80. [18] showed that amorphous polymer material confines during dynamic testing and the confinement delay micro failure mechanisms that cause nucleation in this brittle material and consequently its failure. Their dynamic punching experiments on PMMA showed that this material's confinement might postpone cracking at the benefit of a ductile shear failure mechanism. The punching process produces high hydrostatic pressure. It leads to the tensile failure of brittle polymeric material. It is now well established that brittle materials' confinement may cause dynamic failure by a ductile mechanism. [14] conducted the static and dynamic mechanical performance of cylindrical PMMA subject to compression and showed the rate and pressure sensitivity of this polymer over a various range of strain rates. The quasi-static state demonstrated ductility behaviour. The dynamic failure mode contained axial splitting and confining pressure at lower strain rates and adiabatic shear formation of a conical plug at higher strain rates. In this study, three-dimensional constitutive models were simulated to investigate the mechanical performance of PC and PMMA targets subjected to 0.3" projectile. Ballistic impact of monolithic targets is conducted using numerical simulation under the inclined impact of 30° and normal inclined of 90° to analyse the maximum depth of penetration (DOP) and path of penetration (POP) of the projectile in these amorphous polymers considering various parameters such as; angle of initial velocity, projectile core density, impact velocity. Various experimental analysis performed in literature quantified comparison of target and projectile's damage and penetration is conducted to validate simulated models' accuracy. It is used to investigate the DOP, POP ballistic limit and residual velocity with various projectile core density 7800, and $5850 kg/m^3$ and impact velocity $720, 600, 500, 400, 300 \frac{m}{s}$. The damage and extent of damage are important metrics that must be replicated in an accurate numerical model of bullet-glass interaction. There have been several studies that have quantified damage in glass resulting from impact.

2. Numerical Analysis

3D FE modelling of the target and projectile were simulated using half symmetry, as shown in Fig. 1(a),(b). The target's dimension is $250 \times 50 \times 40 (mm^3)$, and the bullet's radius is $4.8mm$, with an overall length of $35mm$. The target and projectile were meshed using the MultiZone hexahedral method and Automatic method, respectively. A general contact algorithm of ANSYS Workbench is used, and the material's failure controls the erosion.

2.1. Inclined and normal impact of a projectile on target

Numerical analysis of the projectile was simulated considering a simple Von-Mises yield criterion in that the deformation and failure of the kinetic projectile are negligible in a penetration process. The projectile motion and its penetration procedure were analysed given being a rigid-body [8]. 4340 Steel and Copper were comprised in that the strain hardening effects were neglected. Two impact angles 30° and 90° were simulated to investigate the DOP and POP at the targets and illustrated in Fig. 2.

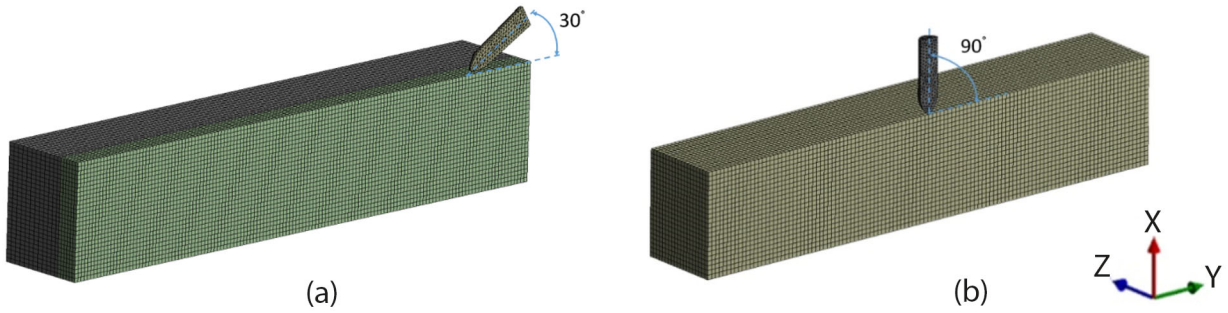

Figure 2: Projectile impacting plate at 30° (a) and 90° (b).

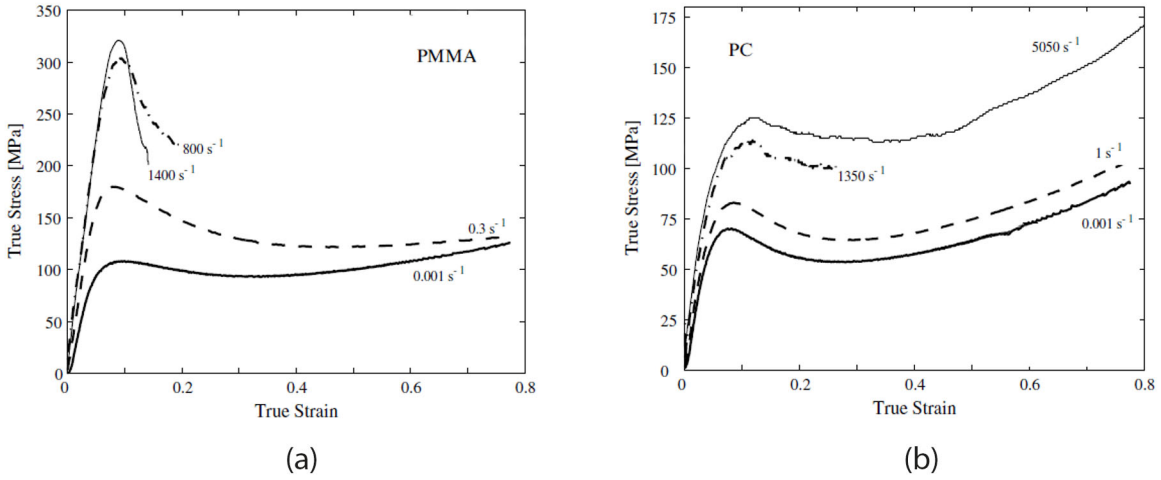

Figure 3: Representative curves of (a) PMMA and (b) PC true stress-strain behaviour in uniaxial compression at four low, moderate, and high strain rates, [11].

2.2. Material model of PMMA and PC

The materials used in this study were two amorphous polymers, polycarbonate (PC) and Polymethylmethacrylate (PMMA). The compressive stress/strain for PC and PMMA at room temperature and over a wide range of strain rates is depicted in Fig. 3. The general form of the response of these polymers is the same over the wide range of temperatures and strain rates, and the dependency on strain rate is minimal [22]. These results are validated with the experimental study presented in [12]. An initial elastic response followed by yielding, strain softening, and a dramatic strain hardening result from adiabatic heating. This adiabatic temperature rise is observable through the large deformation of the samples. In the high rate testing, the PC specimens deformed in a ductile manner over the high strain rates, $1200s^{-1}$ to $4000s^{-1}$ (actual strain rate at yield). The slope of the flow curve decreases (decreasing strain hardening rate) with a strain rate increases. PMMA's strain hardening completely disappears at high strain rates due to the adiabatic heating effects, and for PC, the adiabatic heating has much less impact on the strain hardening rate. The flow stress of PMMA is more temperature-sensitive than that of PC. Therefore thermal softening is apparent in the PMMA. Finite Element simulation of PMMA and PC were conducted using Extended Drucker-Prager Strength (EDP) material model and Hydrodynamic material model with Hugoniots equation of state (Shock EOS Bilinear), respectively.

2.3. Failure Criterion for PMMA and PC

To simulate the high strain rate sensitive polymers (PMMA, PC), ANSYS Workbench explicit Dynamic finite element code was used; the geometry is modelled in AUTODESK INVENTOR. For numerical simulation of PMMA and PC, the effects of two failure criteria (ductility and brittleness) were studied with erosion control and element removal. The failure of brittle materials is a tensile failure, which fractures when the tensile stress reaches fracture strength. Damage initiation in ductile failure is due to nucleation and growth of voids in materials where the equivalent plastic strain at the damage initiation is a function of the stress triaxiality η and plastic strain rate $\dot{\epsilon}$. Triaxial stress, low temperatures, and high strain rates reduce

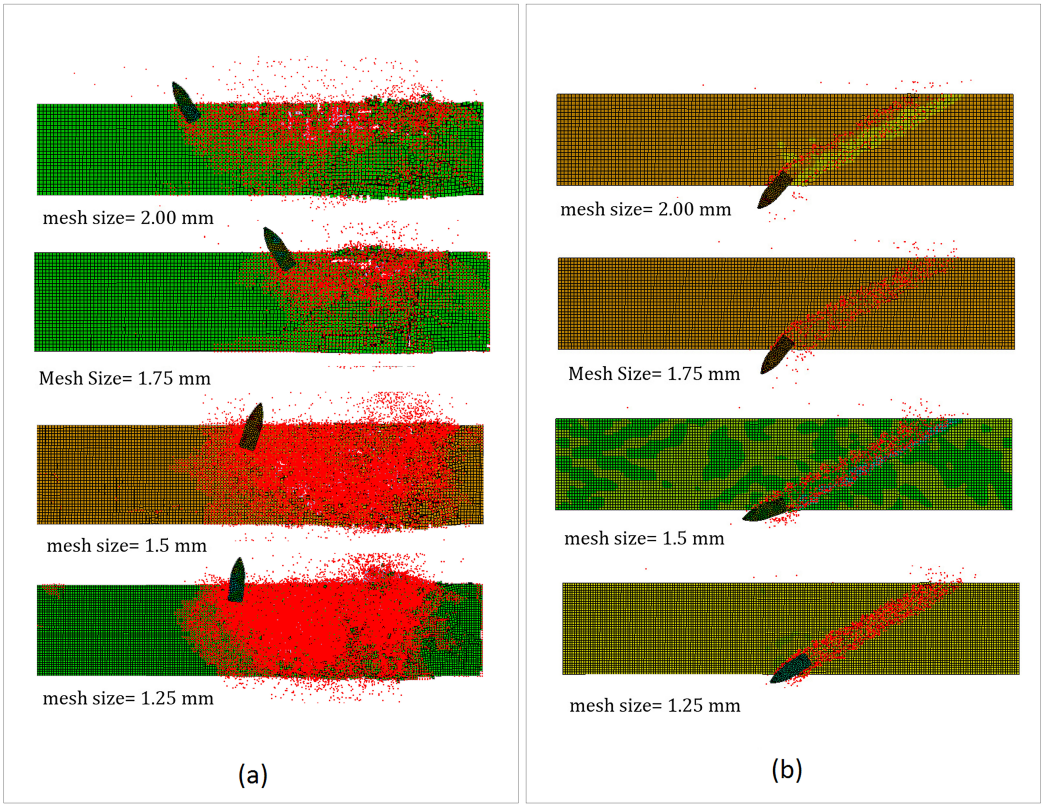

Figure 4: Comparison between PMMA (a) and PC (b) plate's trajectory with different mesh sizes at 30° and after 200μs.

structural material's ductility locally [9]. Stress triaxiality can affect the rupture by preventing plastic deformation and avoid growing inside the material. This study's failure criterion is a plastic strain, tensile pressure, and significant stress failure with element removal choice. When the failure criterion is met at an element integration point, the material point fails and the element is removed. The failure of ductile materials is a shear failure; according to ductility criterion, the material fails if the maximum shear stress reaches the shear strength, [7]. Stress failure and tensile pressure failure were used to simulate the brittleness. Ductility or plastic strain failure depends on triaxiality, strain rate and temperature; thus, the max equivalent plastic strain criterion is used for simulation.

2.4. Mesh sensitivity analysis

Mesh sensitivity analysis was conducted considering various constant mesh sizes; 1, 1.25, 1.50, 1.75, 2.00 *mm*, with 352611, 182931, 121849, 76735, 55736 elements, respectively. The mesh convergence was achieved through an iterative method. Fig. 4 illustrates the trajectory of PMMA and PC with various mesh sizes. The projectile has a velocity of $720\frac{m}{s}$; its density is $7800\frac{Kg}{m^3}$ and the impact angle is 30°. The addition of elements increased the solve time, and the mesh refinement discontinued when the same solution was achieved. The results of stress, deformation, DOP converged to a repeatable solution with decreasing element size. Small red dots in Fig. 4 around the plate show the elements' failure and segmentation. The constant size of the elements throughout the simulation was 1.5*mm* and 1.75*mm* for PMMA and PC, respectively.

3. Numerical simulation and material model of polymethylmethacrylate (PMMA)- Plexiglas

The classic Drucker Prager criterion is a simple modification of the Von-Mises criterion, where the von Mises principle is modified to include hydrostatic stress sensitivity. Although the linear Drucker-Prager yield criterion includes some sensitivity of yielding to the hydrostatic stress, it cannot describe behaviour with any accuracy under stress states in which there is a high component of hydrostatic tension. Drucker Prager (DP) is a pressure-dependent material model that can be used to determine whether a material has failed or undergone plastic yielding. [3] have presented strain gradient plasticity theory based on Drucker-Prager (DP) yield function. The Extended Drucker Prager Strength (EDP) material model is used in this study, representing dynamic tensile failure, the spall strength, and characterising yielding to hydrostatic stress [1, 3]. The

Density ($\frac{Tonne}{mm^3}$)	ρ	$1.18e^{-9}$
Poisson's Ratio	ν	0.42
Shear Modulus (MPa)	G	2300
Sound Velocity ($\frac{mm}{s}$)	C_0	2.57
Frictional Drucker-Prager angle	β	20°
for ($\dot{\gamma} = 10^2$ to $10^4 \frac{1}{s}$), to minimize the thermal effects	ϵ	0.06
Pressure sensitivity for high strain rate	α	0.2436
Reference shear flow stress (MPa)	τ_0	124.2
Tensile stress (MPa)	σ	100-150
Yield stress (MPa)	Y	200-350

Table 1: Material properties of PMMA taken from [14].

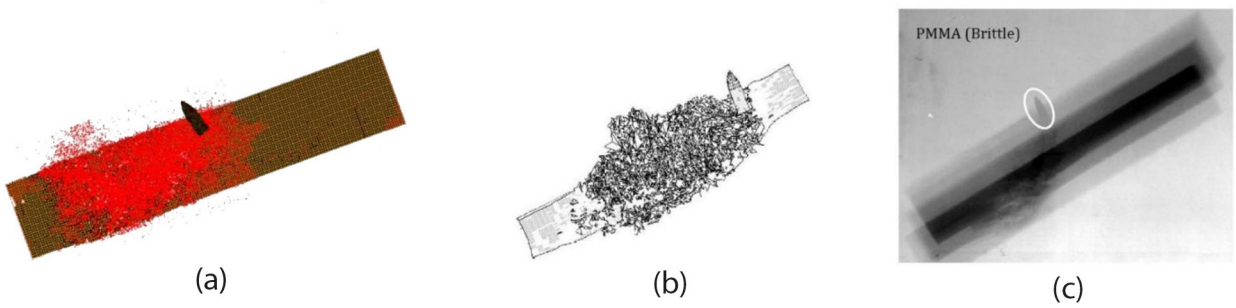

Figure 5: trajectory of the projectile at an obliquity of 30°, in a PMMA plate, (a), Numerical results. (b), (c) Numerical and experimental results (taken from [16]). Note the similarity between the results of the projectile's reflection and penetration.

EDP material model includes three yield criteria and corresponding flow potentials similar to those of the classic Drucker Prager model used for materials with internal cohesion and friction [4]. The yield functions can be combined with anisotropic or kinematic hardening rule to evolve the yield stress during plastic deformation. Eqn.1 can express the rate and pressure dependence of the mechanical behaviour of PMMA at a high strain rate, as follows:

$$\tau_{flow} = 66.78\dot{\gamma}^{0.06933} + \alpha p \tag{1}$$

Where $\tau_{flow} = 0.5\sigma_{flow}$ is the shear flow stress, α is the pressure sensitivity coefficient, $p = \frac{(\sigma_{flow}+2q)}{3}$ is the hydrostatic pressure, and q is the pressure confinement of the material.

The material is known to have a relatively high dynamic compressive strength of around $250MPa$. This relatively high value of compressive strength results from the high strain rates, which PMMA experiences under dynamic loading condition. The material is also too brittle with a spall strength of $100 - 150MPa$ [16] and tensile pressure failure of -5 MPa for. This pressure causes plastic deformation within the PMMA plate that corresponds to a high level of Von Mises stress [15]. This failure is accompanied by a maximum equivalent plastic strain (ϵ_P^{max}), pressure sensitivity index (β) and dynamic yield strength. Table 1 shows the material properties used for the FE simulation of PMMA. Numerical analysis performed in this study was compared with the experimental results to validate the simulation's accuracy. Fig. 5 shows the similarity between the numerical simulation and experimental results for the brittle PMMA. It illustrates that the projectile's orientation and position in the target are well imitated with principal stress and tensile pressure failure at the velocity of $720\frac{m}{s}$. The representative value of $133MPa$ for stress and $-5MPa$ for tensile pressure failure is used throughout this study to simulate the PMMA. The ration of compressive to spall strength failure is around 20. As the ratio of compression to tension increases, the brittleness of the materials rises. The collapse of the target around the impact area in the simulation is similar to the amount of impairment in numerical and experimental results shown in Fig. 5(b), and Fig. 5(c) respectively. The results show a minimum ductile failure related to the yield stress and the dependency of plastic strain failure on the triaxiality. The material's failure happens through plastic deformation, rupture and cracking. The numerical simulation results illustrated that high compressive strength exerts a large asymmetric force on the projectile during the penetration. This force deflects the projectile's flight line towards the outside, making a "flat U Shaped" POP. This asymmetric force on the projectile will continue to act all through the penetration process. Fig. 6 shows the max stress of PMMA target at the velocity of $720\frac{m}{s}$ at an angle 30°. It shows that the target material near the entrance fails due to release waves from the impacting object and continuously exerts the upward push. As shown in Fig. 6, a large section of the target is shattered, followed by large cracks

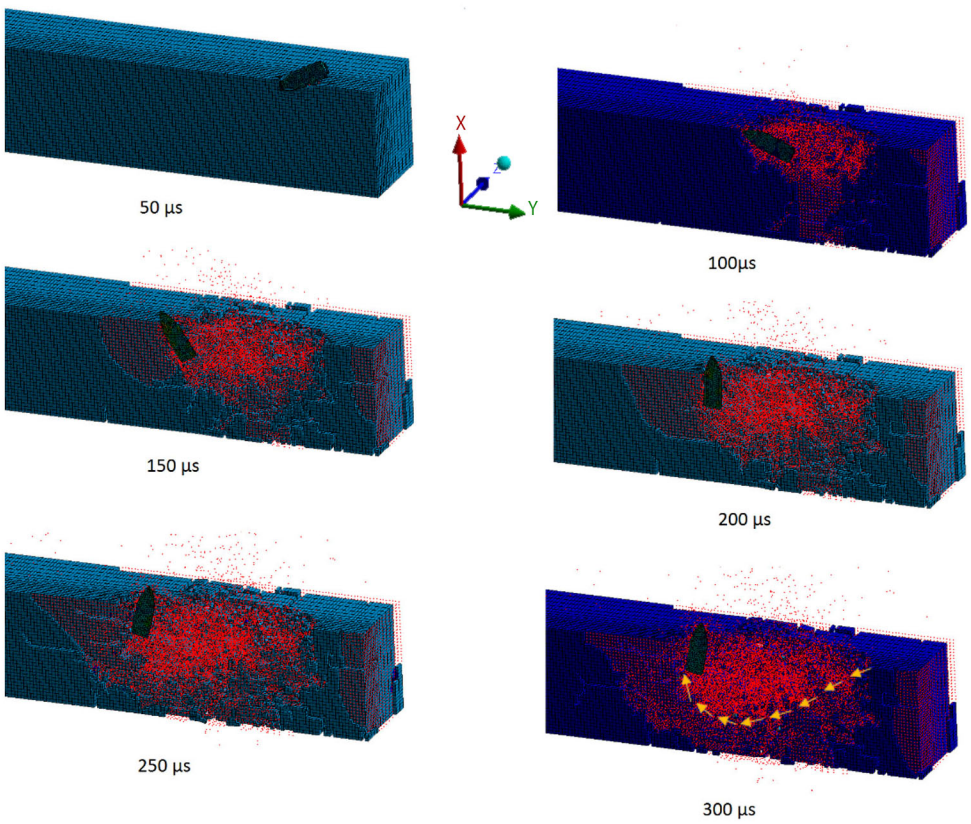

Figure 6: Time evolution of Maximum principal stress of projectile penetration into brittle PMMA plate at the velocity of $720\frac{m}{s}$ and 30°.

and segmentation and, finally, the element's removal. The results demonstrated that the material exerts an upward push on the projectile always; therefore, the projectile does not penetrate more deeply due to the tensile failure, which depends on triaxiality.

3.1. The influence of projectile velocity on PMMA target with 30° *and* 90° *impact*

Numerical simulation of projectile impacting a PMMA plate were carried out considering five initial velocities for projectile: $720\frac{m}{s}$, $600\frac{m}{s}$, $500\frac{m}{s}$, $400\frac{m}{s}$ and $300\frac{m}{s}$. The material properties, geometry, failure criteria, mesh and boundary conditions are remained constant as explained in previous section. The effects of different velocities of projectile on PMMA's trajectory, projectile's reflection as well as DOP and POP were analysed. Fig. 7 shows the effects of projectile's initial velocity on PMMA target at an angle of 30°. It demonstrates that the DOP decreases with the decrease of velocity. The absolute path also seems to change as the impact speed increases by comparing the result for $400\frac{m}{s}$ to those for the higher speeds. In all the models, the target plate cracked and shattered as the projectile penetrated through it. The POP in all the models illustrates that the projectile deflected from its original impact direction with an asymmetric force that oppositely reflects its flight direction with a "U shaped" path. Fig. 8 illustrates the PMMA plate's trajectory with projectile's impact angle of 90° at different initial velocities "720, 600, 500, 400 and $300\frac{m}{s}$" after $120\mu s$. It shows that the DOP of the projectile decreases as the velocity is reduced from $720\frac{m}{s}$ to $600\frac{m}{s}$ as well as from $600\frac{m}{s}$ to $500\frac{m}{s}$ and so on. At $720\frac{m}{s}$ PMMA is completely cracked and shattered and the projectile penetrated the target thoroughly. As shown in Fig. 8 at $720\frac{m}{s}$ impact velocity the projectile exits the plate before $120\mu s$ but at $300\frac{m}{s}$ the material is cracked and ruptured but there is no full penetration. The material near the entrance area is failed with complete perforation, crack propagation and deep penetration as a result of ductile damage and brittleness. By comparing Fig. 7 and Fig. 8, one can see that there is a significant difference between the DOP and POP at two impact angles 30° and 90°. At the 30° angle, there is a continuous upward push that causes the projectile to deflect from its initial impact direction, whereas it is different at 90° impact. DOP at 90°is much greater than 30° also POP at 90° does not have too much deviation from its initial impact angle.

Fig. 9 shows different impact angle and velocities of the projectile and its effect on Von Mises and intensity stress. The stress is decreasing relatively and linearly as the velocity drops. It illustrates that this stress is relatively high at $720\frac{m}{s}$ for both 30° and 90° impact angles, Fig. 9(a) and Fig. 9(b) respectively. The stress is decreasing relatively and linearly as the velocity dropped to $300\frac{m}{s}$. The influence of projectile's core density on PMMA target is investigated in Fig. 10(a). It displays the

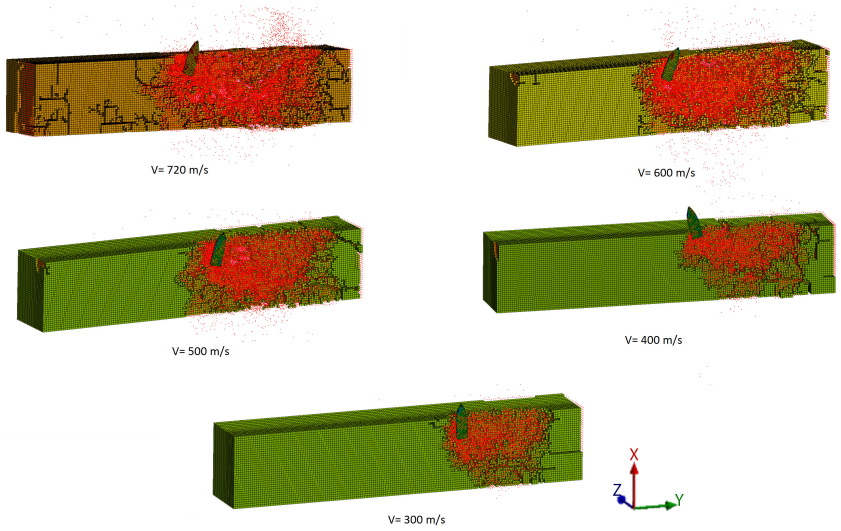

Figure 7: The influence of projectile's velocity on PMMA plate at an angle of 30° (at 300μs after impact).

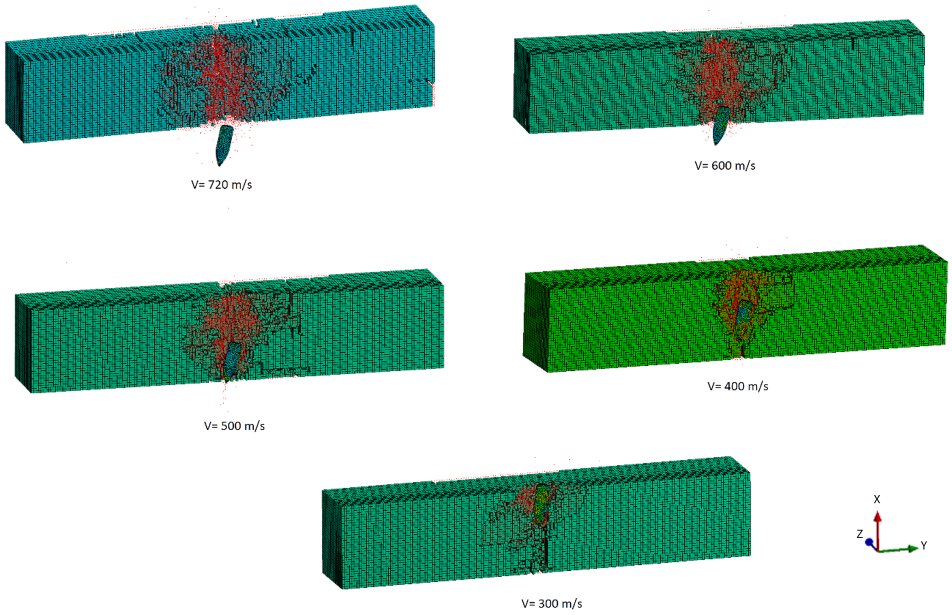

Figure 8: The influence of projectile's velocity on PMMA plate at an angle of 90° (at 120μs after impact).

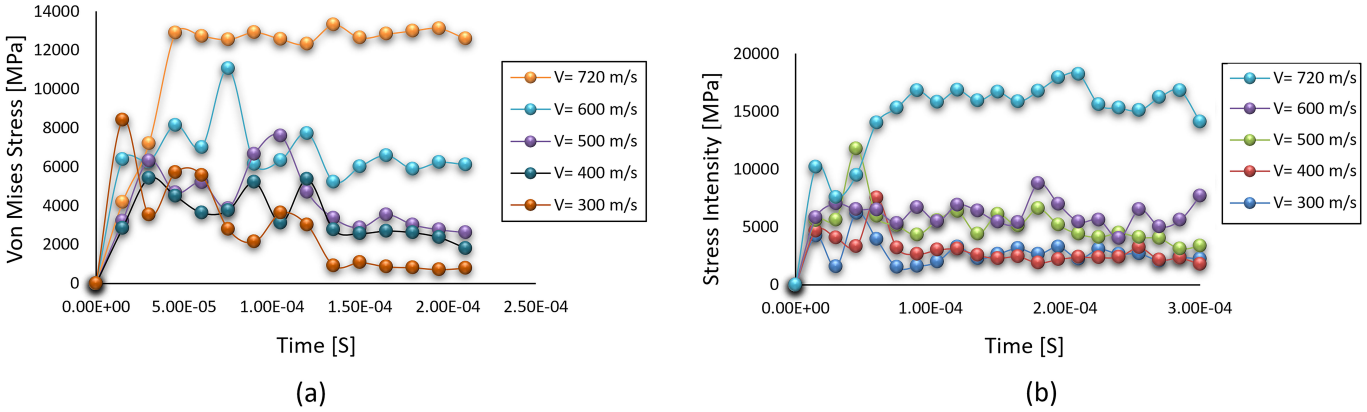

Figure 9: The effects of projectile's velocity on PMMA's Von Mises stress (a) during the projectile's penetration at an angle of 30° (at 350 μs after impact), and (b) 90° (at 120 μs after impact).

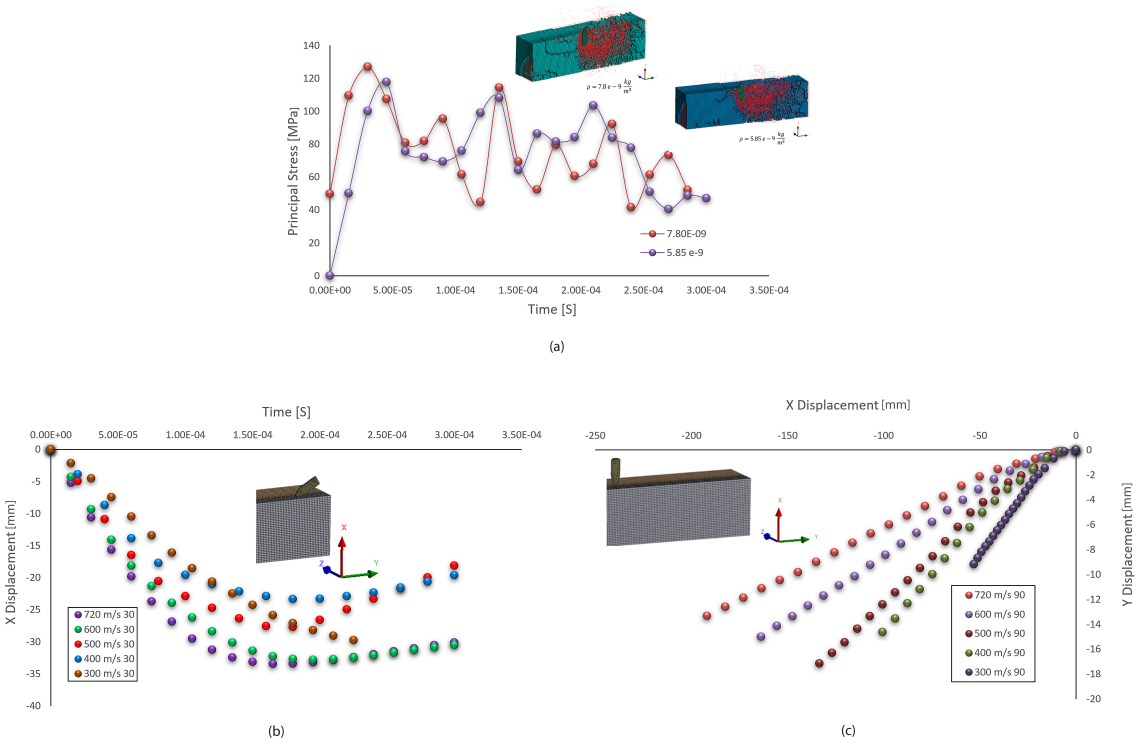

Figure 10: (a) Effects of projectile's core density on max principle stress at 720$\frac{m}{s}$. (b) projectile's displacement through target at different velocity of an angle of 30°. (c) projectile's displacement through target at different velocity at an angle of 90°.

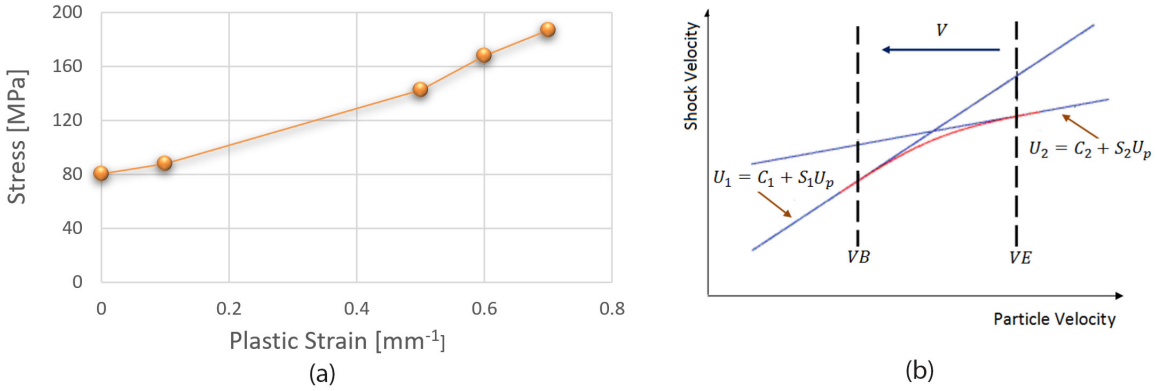

Figure 11: (a) Multilinear Isotropic Hardening (plastic flow) of PC [6]. (b) Shock Velocity and Particle Velocity Relationship.

principal stress of the target at $720\frac{m}{s}$ with two different projectile's core density $7.8e^{-9}Kg/m^3$ and $5.85e^{-9}\frac{Kg}{m^3}$. Projectile with a density of $7.8e^{-9}\frac{Kg}{m^3}$ causes higher stress oscillation which is followed by higher crack and ricochet of the target. Fig. 10(b) demonstrates the projectile displacement along x-axis at various velocities at 30° impact angle. It shows that a push-up follows the displacement along the x-axis, and at $720\frac{m}{s}$, the displacement of the projectile has the highest value. At $400\frac{m}{s}$ after $200\mu s$, the projectile starts to move towards the opposite direction. It is different with $300\frac{m}{s}$ velocity where the projectile does not have enough kinetic energy to move upwards. The kinetic energy and residual velocity of the projectile changes with different velocities, and this value decreases as the projectile velocity decreases.

Fig. 10(c) shows the projectile's displacement through the target at different velocity at an angle of 90° towards the X and Y-direction. The X-direction displacement is much higher than Y-direction, which means the projectile hovers along this direction rather than following a "U Shaped" path.

4. Numerical simulation and material model of Polycarbonate (PC)- Lexan

Polycarbonate is a polymer with high ductility and yield strain with a significant amount of strain hardening that enables it to display impressive impact and perforation resistance [22]. The deformation of PC in a static loading is greater than the dynamic loading since under dynamic loading, and the failure may occur at a more little plastic strain [19]. Experimental observation of PC plate under ballistic impact shows five deformation mechanism for the plate. These mechanisms are dishing, petalling, deep penetration, cone cracking and plugging [22]. A thin PC plate's ballistic impact displays elastic dishing deformation followed by deep penetration, while thick plates demonstrate deep penetration and yawning penetration. Shock Hugoniots equation of state (Shock EOS Bilinear) is more suitable to simulate materials involving compressible shock flows; thus, it is used to simulate PC where its plastic flow is illustrated in Fig. 11(a). Over an extensive range of shock strengths and nonlinearity, two linear fits to the shock velocity and particle velocity relationship must be approximated by a simple fit as shown in Eqn.2, [10, 21]:

$$\begin{cases} U_1 = C_1 + S_1U_P \\ U_2 = C_2 + S_2U_P \end{cases} \tag{2}$$

U_1 is the shock's speed, U_p is the post-shock particle speed, C_1 is the unshocked medium's speed of sound, and S_1 is related to the unshocked medium's isentropic derivative of the bulk modulus concerning pressure. One at low shock compression defined by $U_P > VB$ and one at high shock compression defined by $U_P < VE$ as illustrated in Fig. 11(b).

$$\begin{cases} U = U_1 & V \le VB \\ U = U_2 & V \ge VE \\ U = U_1 + \frac{(U_2-U_1)(V-VB)}{(VE-VB)} & VB < V < VE \end{cases} \tag{3}$$

Mechanical property and hydrodynamic material data of PC over a high strain rate $4900 - 8 \times 10^4 \frac{1}{s}$ is provided in Table2 taken from [5, 10, 22].

PC has higher strain hardening characteristics in tension and compression compared with shear [22]. To validate the numerical simulation in this work, a comparison is performed between numerical simulation and experimental analysis performed by [16, 22]. The experimental and numerical simulation is illustrated in Fig. 12 to display the similarity of the DOP

Density ($\frac{Tonne}{mm^3}$)	ρ	$1.2e^{-9}$
Young's Modulus (MPa)	E	2200
Shear Modulus (MPa)	G	1000
Poisson's Ratio	ν	0.4
Bulk sound Speed ($\frac{mm}{s}$)	C_1	$1.933e^6$
Slope	S_1	2.65
Bulk sound Speed ($\frac{mm}{s}$)	C_2	$2.35e^6$
Slope	S_2	1.6
Gruneisen Coefficient	Γ	0.61
Compressive yield stress (MPa)	σ	100
Equivalent plastic strain	ϵ	4-6%

Table 2: Bilinear shock EOS Material properties and hydrodynamic data for PC

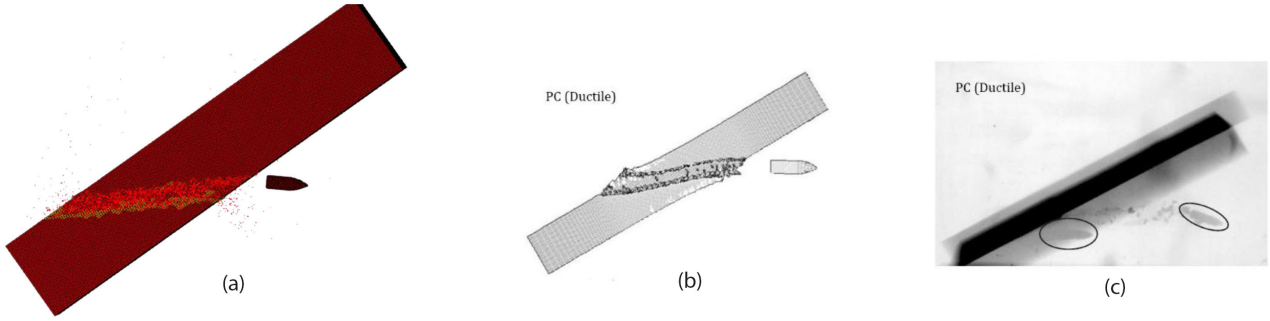

Figure 12: trajectory of the projectile at an obliquity of 30°, the impact velocity of 720$\frac{m}{s}$ in a PC plate, (a), the numerical results. (b) and (c) the reference numerical and X-ray flash experimental result [16].

and its pattern Fig. 12(a). It shows the plate's penetration (embossing of the projectile in the plate without passing through thoroughly) is followed by "S-shaped" perforation (projectile breaking through the plate). The results illustrate that deep penetration occurs in the target with fragments flow around the projectile. It also shows that the cavity diameter in the entrance and exit is larger than the propagation region. The influence of projectile velocity and density on PC target with 30° and 90° impact. The numerical simulation of projectile and PC target is carried out to investigate each parameter's effects on the PC's trajectory. With a spherical projectile, strains are highest below the bullet's nose, and this highly ductile polymer may demonstrate different failure modes than metals do, [19]. The parameters such as velocity and the projectile's core density are changed one by one while the other factors are considered the same (as explained in the previous section). Five different velocity 720$\frac{m}{s}$, 600$\frac{m}{s}$, 500$\frac{m}{s}$, 400$\frac{m}{s}$ and 300$\frac{m}{s}$ is considered at two different impact angles. The material properties, geometry, failure criteria, mesh and boundary conditions remain constant. The projectile perforates the target when its velocity exceeds the ballistic limit or the mean minimum speed for perforation. Fig. 13(a) plots the projectile's DOP at velocities ranging from 300 to 720$\frac{m}{s}$. It can observe the strong sensitivity of the target's trajectory to the projectile's velocity.

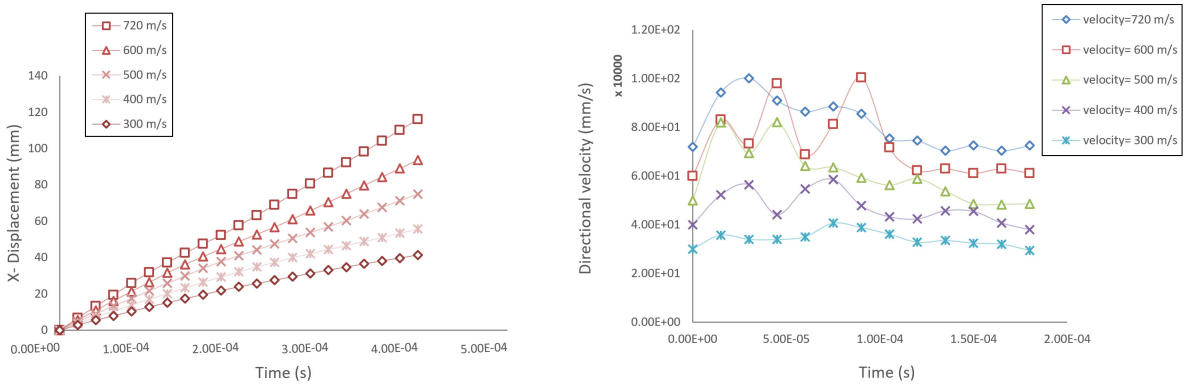

Figure 13: (a) Projectile's DOP at various velocity and an angle of 30°. (b) The directional velocity of the projectile after impacting PC target at 90°.

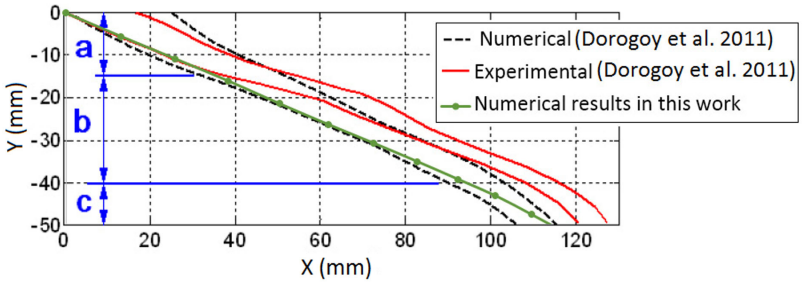

Figure 14: Comparison between numerical and experimental trajectory of target at 30°.

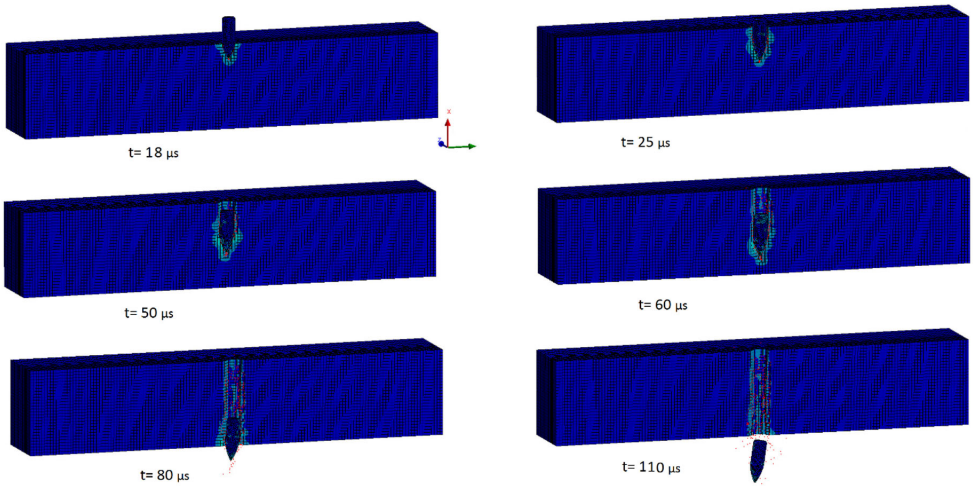

Figure 15: Time evolution of Elastic strain of PC plate at the velocity of 720$\frac{m}{s}$ and 90° impact of the projectile.

The ductile criterion enforces the projectile follow nearly the straight-line path, whereas the tensile test controls the projectile's way. The penetration of PC targets occurs through the axisymmetric force and in-depth penetration process. The results show that the projectile's lower density can lead to less failure of the goal and, finally, less deflection. According to the results, principal stress and plastic strain failure could simulate brittle and ductile characteristic of PMMA and PC plates and yield an acceptable reproduction of experimental results. The PC target with various velocities at normal impact is plotted in Fig. 13(b). It shows the ballistic limit velocity of the plate, which is the critical impact velocity corresponding to a 50% probability of success in defeating the target ($v < v_{50}$). The projectile penetrates and perforates the plate in all the simulated models with different residual velocities relative to its initial velocity. The region around the penetrating projectile undergoes shear yielding as, and PC target changes the reflective index as it yields [22].

The numerical and experimental path of the PC plate at 750$\frac{m}{s}$ is depicted in Fig. 14 that is taken from [2] and compared with numerical results in this work. The numerical data are smoothShear stress of PC target at various velocities and impact angles of 90°.ed and show projectile's movement towards (x,y) direction with three reigns of the trajectory known as a. entrance, b. propagation, and c. exit. A good agreement can be observed for the main characteristics of the trajectory. With all the velocities, the projectile fully penetrated the target, but the penetration takes a longer time to happen as the velocity decreases. This parameter also has significant effects on the DOP since as the velocity decreases, DOP drops. The influence of the projectile's impact angle can be demonstrated through the time progress of elastic strain at 720$\frac{m}{s}$ as shows in Fig. 15. It shows the evolution of projectile deflection and it's penetration at the target. It displays that with 90° impact, POP is "J shape", which is different from 30° which is "S shape". The deflection, which is the angle between the projectile's original direction and the exit direction, is small. The results showed that with an impact angle of 90°, the projectile perforates and exits the target with an orientation nearly parallel to the initial impact angle. The effects of different velocity with 90° impact angle are displayed in Fig. 15. It shows the impact of this factor on penetration depth (DOP) and indicates that DOP scales linearly with the impact velocity. The results also display the deep penetration, and plugging is the failure process of the thick PC.

5. Conclusion and discussion

A comprehensive study of the dynamic failure of monolithic PC and PMMA targets are studied at various impact velocities and projectile's core density with the inclined and normal impact of 30° and 90°. Only half the models were simulated due to the symmetrical nature of the simulated models [16]. The results showed that these two materials could deflect the projectile's course of the flight from its initial angle of penetration. During projectile penetration at $720\frac{m}{s}$ and the oblique impact on PC, projectile follows an "S-shaped" passage with 30° impact, and the maximum stress was $2.29GPa$, whereas PMMA showed a "flat U shaped" POP with a small DOP and maximum stress of $5.16GPa$. PMMA target was entirely shattered and failed, confirming the brittle-ductile characteristic of the material with the residual velocity of $293.8\frac{m}{s}$. The residual velocity of the PC was $244\frac{m}{s}$.
The results showed that the Extended Drucker Prager Strength (EDP) material model with the failure criteria's of principal stress and tensile pressure failure could simulate the PMMA characteristics. It also has been found that these two materials exert a strong asymmetric force on impacting projectile, which results in its strong deflection.
Shock Hugoniots equation of state with plastic strain failure is successfully simulated the specific characteristic of PC target. The results showed that the Extended Drucker Prager Strength (EDP) material model with the failure criteria's of principal stress and tensile pressure failure could simulate the PMMA characteristics. It also has been found that these two materials exert a strong asymmetric force on impacting projectile, which results in its sharp deflection. Shock Hugoniots equation of state with plastic strain failure is successfully simulated the specific characteristic of PC target. The results showed the importance of material properties and their failure criteria, which manages these polymers' brittleness and ductility. The projectile's DOP and POP are affected by the initial impact velocity, the density of the projectile's core projectile, kinetic energy, and the plates. It is also demonstrated that DOP scales linearly with the impact velocity. The results confirmed that PMMA, like other brittle materials, falls into the pressure-induced brittle-ductile transition materials category [2], which indicates that the material strength of PMMA increases with the increase of pressure sensitivity index (β). The projectile's penetration into the target deflects from its original impact axis and stops with an active drag force proportional to its initial velocity value.
Future research will study the possibility of creating a model that can accurately predict the output results of FE analyses of PC and PMMA to describe the behaviour of materials under various loading conditions. The predictive models will be created through Artificial Neural Networks (ANNs) for design optimisation.

Acknowledgement

The authors would like to express their sincere gratitude to the support from the Low Carbon KEEP programme 'European Regional Development Fund (ERDF) - East of England Development Agency' and Essex Safety Glass (ESG) for funding the project.

References

[1] Bardia, P., Narasimhan, R., 2006. Characterisation of pressure-sensitive yielding in polymers. Strain 42 (3), 187–196.

[2] Dorogoy, A., Rittel, D., Brill, A., 2011. Experimentation and modeling of inclined ballistic impact in thick polycarbonate plates. International journal of impact engineering 38 (10), 804–814.

[3] Feng, L., Kang, Y., Zhang, G., Wang, S., 2010. Mechanism-based strain gradient drucker–prager elastoplasticity for pressure-sensitive materials. International journal of solids and structures 47 (20), 2693–2705.

[4] Guide, A., 2005. ANSYS Advanced Analysis Techniques Guide. `http://imechanica.org/files/AdvacedAnsys.pdf`.

[5] Hazell, P., Edwards, M., Longstaff, H., Erskine, J., 2009. Penetration of a glass-faced transparent elastomeric resin by a lead–antimony-cored bullet. International Journal of Impact Engineering 36 (1), 147–153.

[6] Hazell, P. J., Roberson, C. J., Moutinho, M., 2008. The design of mosaic armour: The influence of tile size on ballistic performance. Materials & Design 29 (8), 1497–1503.

[7] Lee, A.-H., 2014. Finite Element Simulations with ANSYS Workbench 15: Theory, Applications, Case Studies. `https://books.google.co.uk/books?id=Zh3GNd9M1oUC&printsec=frontcover&source=gbs_ge_summary_r&cad=0`.

[8] Li, Q., Flores-Johnson, E., 2011. Hard projectile penetration and trajectory stability. International journal of impact engineering 38 (10), 815–823.

[9] Maresca, G., Milella, P., Pino, G., 1997. A critical review of triaxiality based failure criteria. Proc Convegno IGF13 Cassino.

[10] Millett, J., Bourne, N., 2006. Shock and release of polycarbonate under one-dimensional strain. Journal of Materials Science 41 (6), 1683–1690.

[11] Mulliken, A., Boyce, M., 2006. Mechanics of the rate-dependent elastic–plastic deformation of glassy polymers from low to high strain rates. International journal of solids and structures 43 (5), 1331–1356.

[12] Richeton, J., Ahzi, S., Vecchio, K., Jiang, F., Adharapurapu, R., 2006. Influence of temperature and strain rate on the mechanical behavior of three amorphous polymers: Characterization and modeling of the compressive yield stress. International journal of solids and structures 43 (7-8), 2318–2335.

[13] Richeton, J., Ahzi, S., Vecchio, K., Jiang, F., Makradi, A., 2007. Modeling and validation of the large deformation inelastic response of amorphous polymers over a wide range of temperatures and strain rates. International journal of solids and structures 44 (24), 7938–7954.

[14] Rittel, D., Brill, A., 2008. Dynamic flow and failure of confined polymethylmethacrylate. Journal of the Mechanics and Physics of Solids 56 (4), 1401–1416.

[15] Rittel, D., Dorogoy, A., 2014. Impact of thick pmma plates by long projectiles at low velocities. part i: Effect of head's shape. Mechanics of Materials 70, 41–52.

[16] Rosenberg, Z., Surujon, Z., Yeshurun, Y., Ashuach, Y., Dekel, E., 2005. Ricochet of 0.3 ap projectile from inclined polymeric plates. International journal of impact engineering 31 (3), 221–233.

[17] Sarva, S., Mulliken, A. D., Boyce, M. C., Hsieh, A. J., 2006. Mechanics of transparent polymeric material assemblies under projectile impact: simulations and experiments. In: Transformational Science And Technology For The Current And Future Force: (With CD-ROM). World Scientific, pp. 227–234.

[18] Satapathy, S., Bless, S., 2000. Deep punching pmma. Experimental mechanics 40 (1), 31–37.

[19] Shah, Q. H., 2009. Impact resistance of a rectangular polycarbonate armor plate subjected to single and multiple impacts. International Journal of Impact Engineering 36 (9), 1128–1135.

[20] Varghese, A., Batra, R., 2009. Constitutive equations for thermomechanical deformations of glassy polymers. International Journal of Solids and Structures 46 (22-23), 4079–4094.

[21] Ward, G. M., 2011. The simulation of shock-and impact-driven flows with mie-grüneisen equations of state. Ph.D. thesis, California Institute of Technology.

[22] Wright, S., Fleck, N., Stronge, W., 1993. Ballistic impact of polycarbonate-an experimental investigation. International Journal of Impact Engineering 13 (1), 1–20.